Research Letter **DOI:** 10.15541/jim20240410

Enhanced Performance of $La_{0.7}Sr_{0.3}FeO_{3-\delta}$ Cathode for SOFC *via* Implementation of B-site High-entropy Strategy

LIU Hongming[1], ZHANG Jinke[2], CHEN Zhengpeng[1], LI Mingfei[1], QIAN Xiuyang[1], SUN Chuanqi[1], XIONG Kai[3], RAO Mumin[1], CHEN Chuangting[1], GAO Yuan[2], LING Yihan[2]

(1. Guangdong Energy Group Science and Technology Research Institute Co., Ltd., Guangzhou 510000, China; 2. School of Materials Science and Physics, University of Mining and Technology, Xuzhou 221116, China; 3. Guangdong Energy Group Co., Ltd., Guangzhou 510000, China)

Abstract: As classical cathode materials of solid oxide fuel cell (SOFC), Fe-based perovskite materials are favored for their affordable price, low thermal expansion coefficient and high stability. In this study, B-site high-entropy perovskite oxide $La_{0.7}Sr_{0.3}(FeNiCo)_{0.8}Mo_{0.1}Ti_{0.1}O_{3-\delta}$ (LSFNCMT) was prepared by the citric acid-nitrate combustion method. Due to the faster oxygen surface exchange rate of the high-entropy material, the LSFNCMT cathode shows excellent oxygen reduction reaction (ORR) activity with a polarization impedance (R_p) of 0.11 Ω·cm^2 at 800 ℃, which is much lower than that of the $La_{0.7}Sr_{0.3}FeO_{3-\delta}$ (LSF) cathode (0.31 Ω·cm^2). Furthermore, the high-entropy material exhibits superior stability due to incorporation of highly acidic Ni, Co, and Mo cations as well as Ti cation with more negative average bonding energy (ABE) of metal-oxygen. In the 22 h-stability test of the symmetric cell with LSFNCMT cathode in the Cr-containing atmosphere, R_p only increases from 1.07 Ω·cm^2 to 2.98 Ω·cm^2, while R_p of the LSF cathode increases from 2.62 Ω·cm^2 to 7.90 Ω·cm^2 under the same conditions, indicating better Cr-resistance of LSFNCMT due to the high-entropy strategy. The fact that the maximum power density (MPD) of the single cell with LSFNCMT cathode at 800 ℃ is 1105.26 mW·cm^{-2}, significantly higher than that of LSF cathode (830.74 mW·cm^{-2}), and R_p at 800 ℃ is 0.24 Ω·cm^2, lower than that of LSF cathode (0.36 Ω·cm^2), confirming excellent toxicity resistance of the high-entropy cathode. This study shows that B-position high entropy is an effective way to improve the catalytic activity and chromium resistance of cathode materials.

Key words: solid oxide fuel cell; cathode material; B-site high entropy; anti-chromium poisoning

SOFC is a promising energy conversion system that can directly convert the chemical energy in the fuel into electrical energy, and this process is characterized by high efficiency and low pollution[1-5]. Traditional SOFCs run at ~1000 ℃, causing cathode material degradation and sealing problems, and greatly limiting the commercialization of SOFCs[6]. Therefore, reducing the operating temperature of the cell is an inevitable trend in the development of SOFC[7-11]. However, with the decrease in operating temperature, the electrochemical activity of the cathode material decreases, leading to the reduced electrochemical performance of the cell[12]. Therefore, the research focus of SOFC development lies in the advancement of cathode materials with exceptional catalytic activity at medium and low temperatures.

In recent years, the research on cathode materials mainly focuses on perovskite oxides, including single perovskite, double perovskite and perovskite-like oxides that possess excellent ionic and electron mixed conductivity[13-16]. ABO_3 perovskite materials have attracted much attention due to their abundant oxygen vacancy content, which can provide a variety of conductance mechanisms[17-19]. Among them, Fe-based

Received date: 2024-09-14; **Revised date:** 2024-12-11; **Published online:** 2024-12-27
Foundation item: Key-Area Research and Development Program of Guangdong Province (2022B0111130004); National Natural Science Foundation of China (52272257)
Biography: LIU Hongmin (1996–), male, PhD. E-mail: liuhongming@geg.com.cn
刘弘明(1996–), 男, 博士. E-mail: liuhongming@geg.com.cn
Corresponding author: GAO Yuan, post doctor. E-mail: tbh371@cumt.edu.cn; LING Yihan, professor. E-mail: lyhyy@cumt.edu.cn
高 源, 博士后. E-mail: tbh371@cumt.edu.cn; 凌意瀚, 教授. E-mail: lyhyy@cumt.edu.cn

perovskite materials have competitive price and low thermal expansion coefficient, which perfectly matches electrolyte and connector of SOFCs, showing promising development prospects as cathode materials at low temperatures[7, 17, 20-22]. Therefore, extensive researches have been conducted on Fe-based perovskite cathode materials, including $La_{0.7}Sr_{0.3}FeO_{3-\delta}$ (LSF)[23], $La_{0.6}Sr_{0.4}Co_{0.2}Fe_{0.8}O_{3-\delta}$ (LSCF)[24] and $La_{0.6}Ce_{0.1}Sr_{0.3}Fe_{0.95}Ru_{0.05}O_{3-\delta}$ (LCSFR)[25]. In addition, in practice the chromium in the connector material of SOFC inevitably volatilizes and spreads into the environment, easily reacting with the alkaline earth metal cations segregated on the cathode surface, generating inert phases and seriously degrading the cell[26-28]. Jiang *et al*.[29] found that the $La_{0.6}Sr_{0.4}Co_{0.2}Fe_{0.8}O_{3-\delta}$ electrode reacted with chromium on the electrode surface to form insulating phases in the chromium vapor environment, such as $SrCrO_4$ and Co_3O_4, resulting in increased R_p. Therefore, the stability of iron-based perovskite cathode materials in chromium-containing environments is critical for practical applications.

More recently, high-entropy oxides have attracted great attention due to their excellent physical and chemical properties, such as high thermal stability, unique magnetic properties, high-efficiency lithium-ion storage properties, great dielectric properties and excellent catalytic properties[18, 30-33]. High-entropy oxides are oxides with a single structure obtained by the solid solution of five or more kinds of metal or non-metal oxides in equal or similar molar ratio. Due to the wide selectivity of constituent elements and contents, high-entropy perovskite oxides have many novel functional properties and infinite possibilities. For example, Gao *et al*.[31] designed a medium-entropy $Sr_{1-x}Co_{0.5}Fe_{0.2}Ti_{0.1}Ta_{0.1}Nb_{0.1}O_{3-\delta}$ (S_{1-x}CFTTN, x=0–0.15) oxide that exhibited both excellent ORR activity and chromium resistance. Han *et al*.[34] synthesized $La_{0.2}Pr_{0.2}Nd_{0.2}Sm_{0.2}Gd_{0.2}BaFe_2O_{5-\delta}$ (LPNSGBF) from $PrBaFe_2O_{5-\delta}$ as SOFC cathode, showing excellent chromium resistance. For perovskite cathode materials, the catalytic activity is determined by the B-site ion's activity, and the presence of uniformly dispersed transition metals on the B-site offers abundant valence variability thereby facilitating enhanced ORR activity[35-36]. Recently, it was found that doping more stable elements in the B-site of perovskite can improve the structural and chemical stability of materials in oxidizing atmospheres[30, 37-39]. For example, replacing Co or Fe ions in perovskite with Ti^{4+} ions can effectively reduce the coefficient of thermal expansion and improve the stability of material[40-41].

Based on the inspiration from previous studies, this work utilizes high-entropy effect to optimize the catalytic activity and chromium resistance of traditional Fe-based materials. B-site high-entropy perovskite oxide $La_{0.7}Sr_{0.3}(FeNiCo)_{0.8}Mo_{0.1}Ti_{0.1}O_{3-\delta}$ (LSFNCMT, Sconfig=1.51R) was synthesized by uniformly doping a variety of transition metals at the B-site, and the entropy calculation method has been described in our previous work[31]. In particular, the solid solution limit of the elements Mo and Ti restricts the maximum solubility to no more than 10% (in molar) in the LSF material. The structural characteristics, compatibility, electrochemical performance and stability of the material under chromium-containing atmosphere were studied systematically.

1 Experimental

1.1 Preparation of LSF and LSFNCMT

LSF and LSFNCMT powders were prepared by the citric acid-nitrate combustion method. According to the stoichiometric ratio, La_2O_3, $Sr(NO_3)_2$, $Fe(NO_3)\cdot 9H_2O$, $NiC_4H_6O_4\cdot 4H_2O$, $Co(NO_3)_2\cdot 6H_2O$, $(NH_4)_6Mo_7O_{24}\cdot 4H_2O$ and $C_{16}H_{36}O_4Ti$ were dissolved in nitric acid (metal compounds : nitric acid=1 : 1 (in molar)), and citric acid and ethylenediamine tetraacetic acid (EDTA) were added according to citric acid : EDTA : metal ion=0.8 : 1 : 1 (in molar). The solution was stirred and heated on the magnetic stirrer until it became clear. Then, an appropriate amount of $NH_3\cdot H_2O$ was added to regulate the solution to pH 7, and stirred until spontaneous combustion occurred. The obtained powder precursor was calcined at 1050 ℃ for 5 h to afford LSFNCMT powder. LSF was prepared by the same method. Other powders such as NiO, $Zr_{0.85}Y_{0.15}O_2$ (YSZ) and $Gd_{0.1}Ce_{0.9}O_{2-\delta}$ (GDC) are commercially available (SOFCMAN).

1.2 Fabrication of SOFC

For symmetric cell, 0.25 g of GDC powder was ball milled and pressed into a finished disc at 200 MPa, then calcined in air at 1450 ℃ for 6 h. The resulting GDC electrolyte pellet was then polished to a uniform thickness. Before the addition of 2 g of 10% (in mass) terpineol ethyl cellulose, 1 g of LSF/LSFNCNMT powder was ground for 30 min. The slurry was ground for another 2 h to afford the cathode slurry. Finally, LSF and LSFNCMT slurry were uniformly coated on

both sides of the GDC electrolyte sheet by screen printing method, and calcined at 1000 ℃ for 3 h to afford the symmetric cell LSF|GDC|LSF and the symmetric cell LSFNCMT|GDC|LSFNCMT with the cathode effective areas of 0.24 cm^2.

The anode support of single cell was prepared by the dry pressing method. NiO-YSZ anode powder was prepared by ball milling with NiO, YSZ and starch as raw materials according to a mass ratio of 6 : 4 : 3. In this process, alcohol was used as ball milling medium and polyester/polyamine copolymer (KD-1) as dispersing agent. 0.4 g of dried NiO-YSZ powder was pressed into ϕ15 mm anode substrate. The anode substrates were sintered at 1000 ℃ for 3 h to afford the anode support body. 10 g of YSZ powder was ball milled with 2% (in mass) KD-1 dispersant, 20 g of 5% (in mass) terpineol ethyl cellulose and 25 g of acetone for 24 h to afford the electrolyte slurry. Electrolyte films were prepared by the spin-coating method. YSZ slurry was spin-coated on NiO-YSZ anode substrate for 3 times at 6000 r/min, and then sintered at 1400 ℃ for 10 h to prepare the NiO-YSZ|YSZ half cell. A GDC buffer layer was further added between the electrolyte and the cathode. The preparation process of GDC paste is the same as that of YSZ paste above. The GDC slurry was uniformly spin-coated on the surface of YSZ at 5000 r/min for 30 s, and sintered in air at 1300 ℃ for 3 h to afford the barrier layer. The cathode paste was coated on the surface of the barrier layer by the screen-printing method, and then calcined in air at 1000 ℃ for 3 h to afford single cells NiO-YSZ|YSZ|GDC|LSF and NiO-YSZ|YSZ|GDC|LSFNCMT with effective cathode areas of 0.24 cm^2.

1.3 Characterization

The phase structure of the cathode powder and its chemical compatibility with the electrolyte were characterized by X-ray diffractometer (XRD, Bruker 8 Advance) at room temperature within 2θ=20°–80°. Scanning electron microscopy (SEM) was used to analyze the morphology of cathode materials and cells, and energy dispersive spectroscopy (EDS, Oxford Instrument Aztec Energy) was used to analyze the distribution of elements in the samples. The electrochemical performance, including current–voltage (I–V), electrochemical impedance spectroscopy (EIS) and steady-state voltage, was tested using an electrochemical workstation (IM6, Zahner). The electrochemical process of the cell was analyzed by the relaxation time distribution (DRT) according to the range of characteristic frequency of EIS data.

2 Results and discussion

2.1 Phase structure, microstructure and chemical compatibility

XRD patterns of the cathode materials LSF, LSFNCMT and the standard $LaFeO_3$ (PDF#75-0439) are shown in Fig. 1. Both materials possess single perovskite structure, and no second phase is detected (Fig. 1(a)). After doping with B-site elements, the main peak of LSF moves toward higher angle (Fig. 1(b)), which is attributed to the disparity between the ionic radius of the doped element and that of the B-site cation, resulting in a contraction within the lattice structure of the material.

In order to achieve chemical compatibility between cathode material and electrolyte, cathode material was mixed with electrolyte YSZ and GDC at a mass ratio of 1 : 1 and calcined at 1000 ℃ for 10 h. The impurity peaks of calcined LSF-YSZ and LSFNCMT-YSZ in XRD patterns (Figs. 2(a, b)) indicate the occurrence of a phase reaction between the cathode material and the YSZ electrolyte. XRD patterns of LSF-GDC and LSFNCMT-GDC powders (Figs. 2(c, d)) exhibit a physical superposition of diffraction peaks corresponding to LSF and GDC (Fig. 2(c)), as well as LSFNCMT and

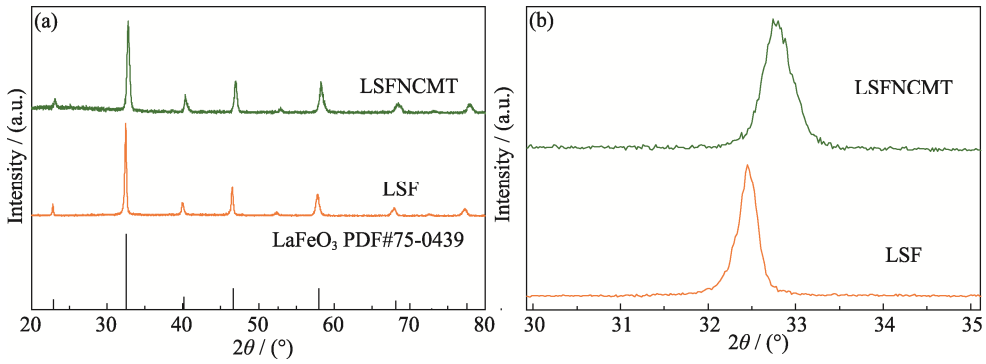

Fig. 1　XRD patterns of (a) LSF, LSFNCMT and $LaFeO_3$ (PDF#75-0439) samples; (b) Local zoom of main peaks

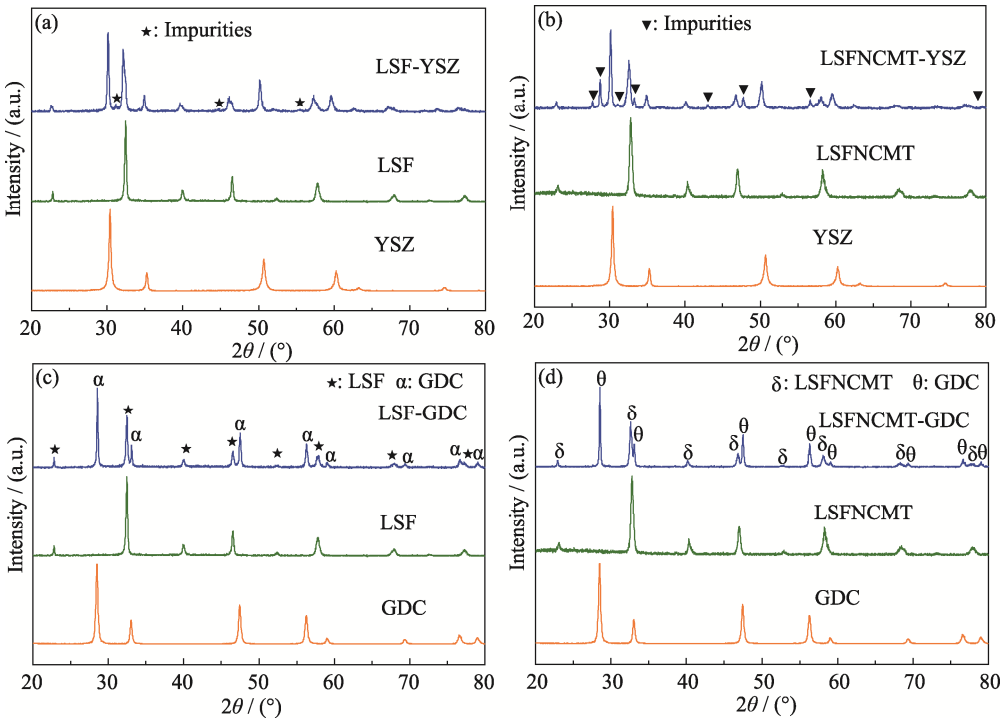

Fig. 2 XRD patterns of mixture of electrolyte materials YSZ with LSF (a) and LSFNCMT (b) and GDC with LSF (c) and LSFNCMT (d)

GDC (Fig. 2(d)), without any new impurity peaks. Therefore, it is imperative to incorporate a GDC barrier layer between YSZ electrolyte and the prepared cathode material. Fig. S1 shows the microscopic morphology of LSFNCMT powder. In SEM image of the LSFNCMT sample sintered at 1050 ℃ for 10 h (Fig. S1(a)), the particles are homogeneously distributed. In EDS spectra of LSFNCMT (Fig. S1(b)), La, Sr, Fe, Ni, Co, Mo, Ti and O distribute uniformly without any segregation.

2.2 Electrochemical properties

Fig. S2 and Fig. 3(a) show EIS spectra measured at 650–800 ℃ for symmetric cells prepared with LSF and LSFNCMT materials, respectively. To investigate the impact of high entropy at the B-site on R_p of the cathode material, Figs. 3(a, b) and Fig. S2 are presented with the Ohmic impedance (R_o) of the symmetric cell eliminated. R_p of the LSF symmetric cell at 650, 700, 750 and 800 ℃ are 5.01, 2.00, 0.77 and 0.31 Ω·cm^2, respectively (Fig. 3(c)). Conversely, R_p of the LSFNCMT symmetric cell are only 1.21, 0.49, 0.22 and 0.11 Ω·cm^2 at the same temperatures, indicating enhanced ORR activity of the LSFNCMT electrode. Fig. 3(d) shows R_p and corresponding Arrhenius curves of both electrodes. The activation energy (E_a) of two cathode materials was obtained by slope calculation. The fact that E_a for LSFNCMT is 124 kJ·mol^{-1}, which is 18.4% lower than that of LSF (152 kJ·mol^{-1}), indicating that LSFNCMT cathode material possesses a lower oxygen exchange energy barrier, which is beneficial for the oxygen exchange kinetics and ORR activity of high-entropy material, as confirmed by EIS tests below.

The mechanism of ORR on the oxygen electrode and its rate-limiting steps are further clarified by EIS tests and corresponding DRT diagrams under different oxygen partial pressures ($p(O_2)$, N_2/O_2 mixture). Fig. 4(a) and Fig. S3 show EIS spectra of LSFNCMT and LSF cathodes under different $p(O_2)$ at 700 ℃, respectively. R_p of the cathode increases as the $p(O_2)$ decreases from 2.1×10^4 Pa to 1×10^3 Pa, indicating a strong correlation between the catalytic activity and the oxygen concentration. Due to the fact that ORR is a process of oxygen dissociation/adsorption and bulk oxygen diffusion, R_p is dependent on $p(O_2)$. To distinguish the rate-limiting step in ORR process, DRT analysis is further performed (Figs. 4(b, c)), revealing three distinct peaks at low frequency (LF), intermediate frequency (IF) and high frequency (HF) reaction processes. In Fig. 4(c), DRT results show that the resistance of the high-entropy electrode in the LF, MF and HF regions is significantly less than that of LSF, indicating faster oxygen surface exchange rate of the high-entropy electrode. According to the relationship between R_p and oxygen partial pressure:

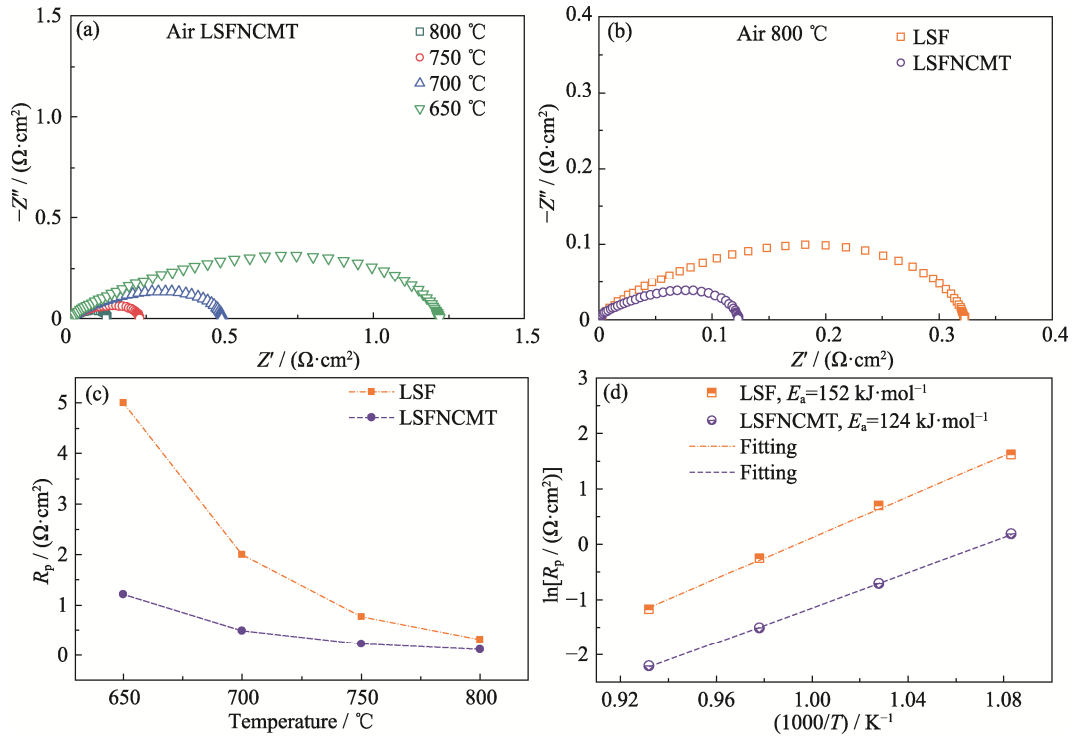

Fig. 3　Electrochemical performance of symmetric cell under different temperatures in air

(a) EIS spectra of LSFNCMT electrode; (b) EIS spectra of LSF and LSFNCMT electrodes at 800 ℃; (c) R_p and (d) corresponding Arrhenius plots of two symmetric cells

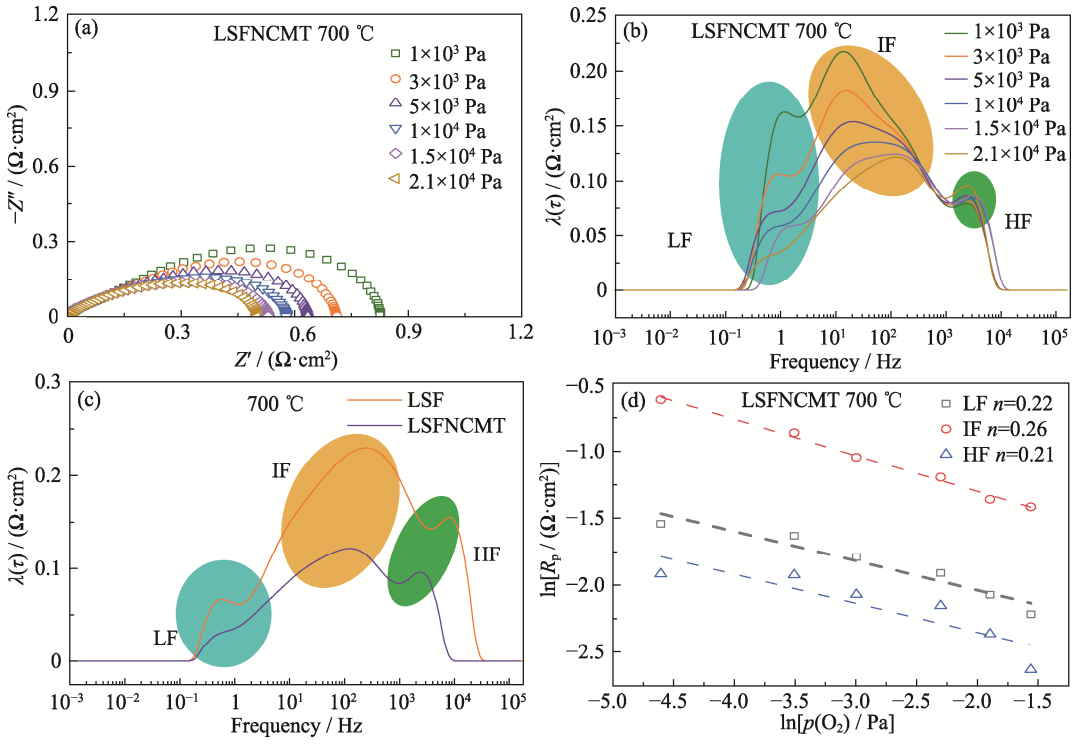

Fig. 4　Electrochemical performance of symmetrical cell under different $p(O_2)$ at 700 ℃

(a, b) EIS spectra (a) and DRT curves (b) of LSFNCMT; (c) DRT curves of LSF and LSFNCMT under $p(O_2)$ of 2.1×10^4 Pa at 700 ℃; (d) Dependence of each R_p as a function of $p(O_2)$ for LSFNCMT. Colorful figures are available on website

$R_p=k(p(O_2))^{-n}$, the value of the reaction order (n) corresponding to R_p is calculated to determine the main rate-limiting step of ORR[42]. The electrode reaction at the cathode encompasses intricate processes, with the n values corresponding to distinct electrochemical reaction processes. Fig. 4(d) shows n

values corresponding to HF, IF and LF under different $p(O_2)$ are 0.21, 0.26 and 0.22, respectively. Among them, n=0.21 (HF) is related to the transfer of O^{2-} across the electrode–electrolyte interface[43], n=0.26 (IF) is related to the dissociation of O_2 to $2O_{ads}$ and O_{ad} to O_{ad}^{-1}[42], and n=0.22 (LF) is related to the adsorption/desorption of oxygen and ionic diffusion of oxygen on the bulk/surface[44]. The high-frequency region remains relatively constant as $p(O_2)$ decreases, while the MF/LF region gradually increases (Fig. 4(b)). This observation suggests that the rate-limiting steps of the ORR process in LSFNCMT are associated with oxygen dissociation, electron transfer and mass transfer.

2.3 Cr-tolerance and stability of half-cells

In the practical application of SOFCs, the volatilization of chromium in the connection material leads to the reaction between Sr/Ba-containing cathode materials and chromium vapor, resulting in the formation of an insulating layer and subsequent cell degradation. This phenomenon, known as chromium poisoning, primarily occurs due to the interaction between nucleating agents and chromium vapors that readily separate at the surface and react with each other[45-46]. The stability and chromium resistance of the LSF and LSFNCMT cathodes are assessed by the variation in R_p under a cathode current density of –200 mA·cm^2, an operating temperature of 700 ℃ and a flow rate of ambient air of 30 mL·min^{-1}. EIS spectra of LSF cathode and LSFNCMT cathode in the presence of Cr_2O_3 are shown in Fig. S4(a) and Fig. 5(a). The presence of Cr vapor significantly deteriorates the performance of LSF cathode (Fig. S4(b)), as evidenced by the notable increase in R_p for both Cr-LSF cathodes (from 2.62 Ω·cm^{-2} to 7.90 Ω·cm^{-2}), suggesting a decline in ORR activity due to the presence of Cr_2O_3. However, it is worth noting that the LSFNCMT cathode (Fig. 5(b)) exposed to Cr_2O_3 exhibits relatively lower increase in R_p (from 1.07 Ω·cm^{-2} to 2.98 Ω·cm^{-2}), indicating improved chromium resistance due to high-entropy doping at the B-site of the LSF cathode. On the one hand, Ti–O bond in LSFNCMT possesses a more negative ABE than Fe–O bond, suggesting that Ti–O bond is stronger than Fe–O bond[30]. Therefore, it is beneficial to replace Fe with Ti for the stability of the material. On the other hand, Ni, Co and Mo cations possess higher acidity than Fe cation at the same valence[47]. Thus, under a Cr-containing atmosphere, these cations are less likely to react with highly acidic Cr vapors, which is conducive to the stability of the material.

2.4 Performance of single cells

I–V curves and power density curves for the single cells using LSF and LSFNCMT cathodes with wet H_2 as fuel and air as oxidant are illustrated in Fig. S5 and Fig. 6(a), respectively. The MPD of the single cell using LSFNCMT cathode remarkably increases by 33.13% (in volume) at 800 ℃, compared to the cell using LSF cathode (Fig. 6(b)). The superior electrochemical performance of LSFNCMT cathode is attributed to its enhanced ORR activity. The open circuit voltage (OCV) of the single cells decreases with the temperature increasing (Fig. 6(c)). At 800 ℃, OCV of the single cell with LSFNCMT cathode is 1.072 V, close to the theoretical value under these conditions, indicating effective sealing of the cell. MPDs of Ni-YSZ|YSZ|GDC|LSF single cell are 159.62, 305.86, 530.93 and 830.74 mW/cm^2 at 650, 700, 750 and 800 ℃ (Fig. 6(d)). MPDs of the Ni-YSZ|YSZ|GDC|LSFNCMT single cell at 650, 700, 750 and 800 ℃ are 242.18, 425.74, 666.08 and 1105.26 mW/cm^2, respectively. The high-entropy doping at the B-site facilitates the kinetics of oxygen migration, thereby augmenting the electrochemical performance. EIS spectra of two single cells in the open circuit state are presented in Fig. S6 and Fig. 7(a), respectively. Impedances for both cells decrease with

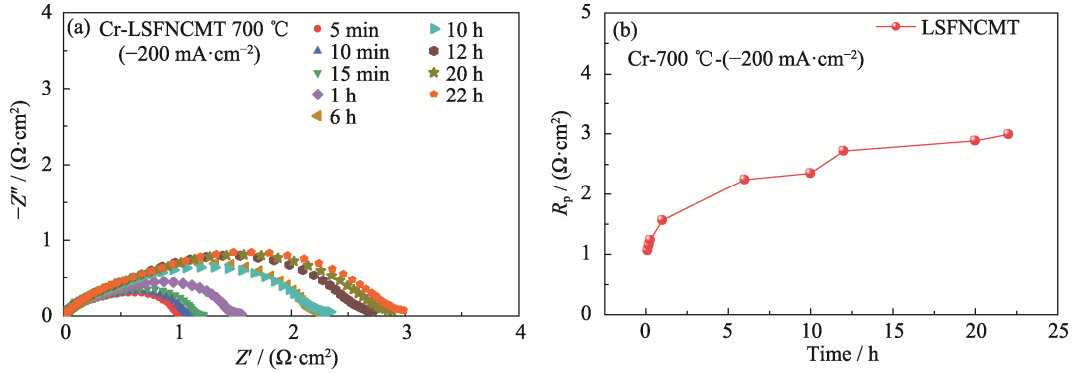

Fig. 5 EIS spectra (a) and variation of R_p (b) of LSFNCMT symmetric cell within 22 h in Cr vapor at –200 mA·cm^{-2} and 700 ℃

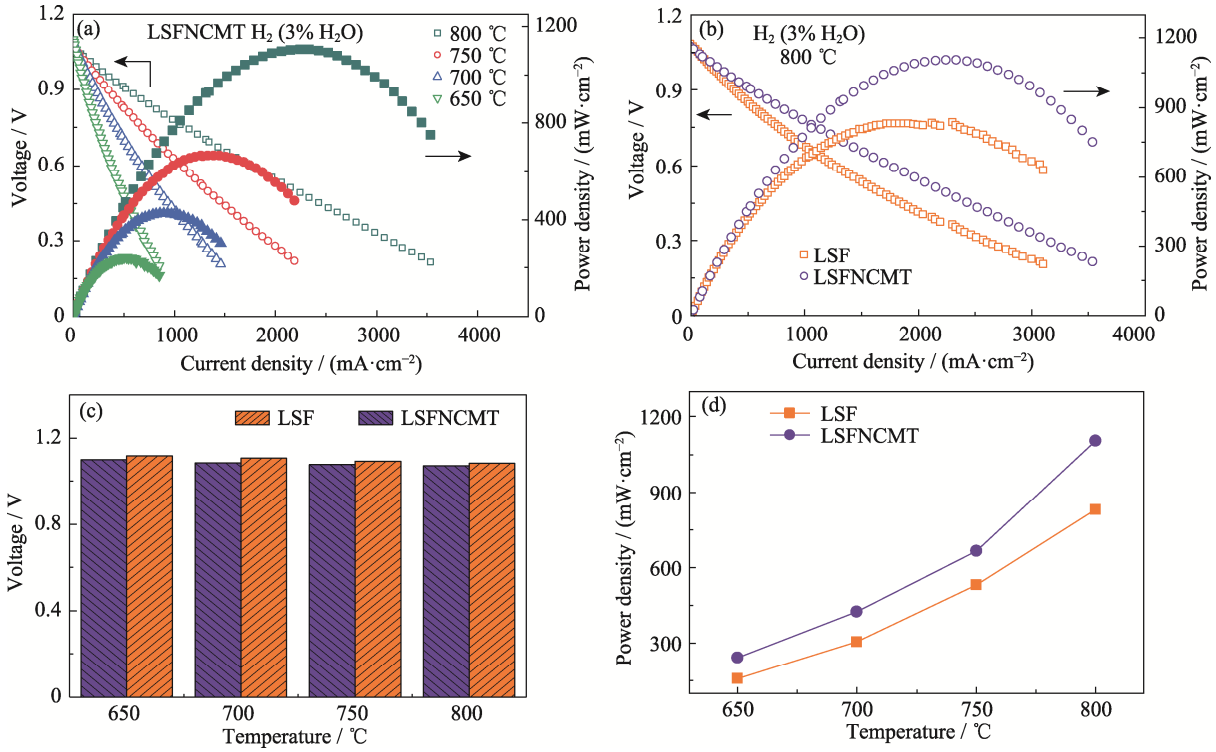

Fig. 6　Electrochemical performance of the single cell at 650–800 ℃ in wet H_2 (3% (in volume) H_2O)
(a) *I–V* and power density curves of LSFNCMT cathodes; (b) *I–V* and power density curves of LSF and LSFNCMT cathodes at 800 ℃; (c) OCV and (d) MPD varied with temperature of different single cells

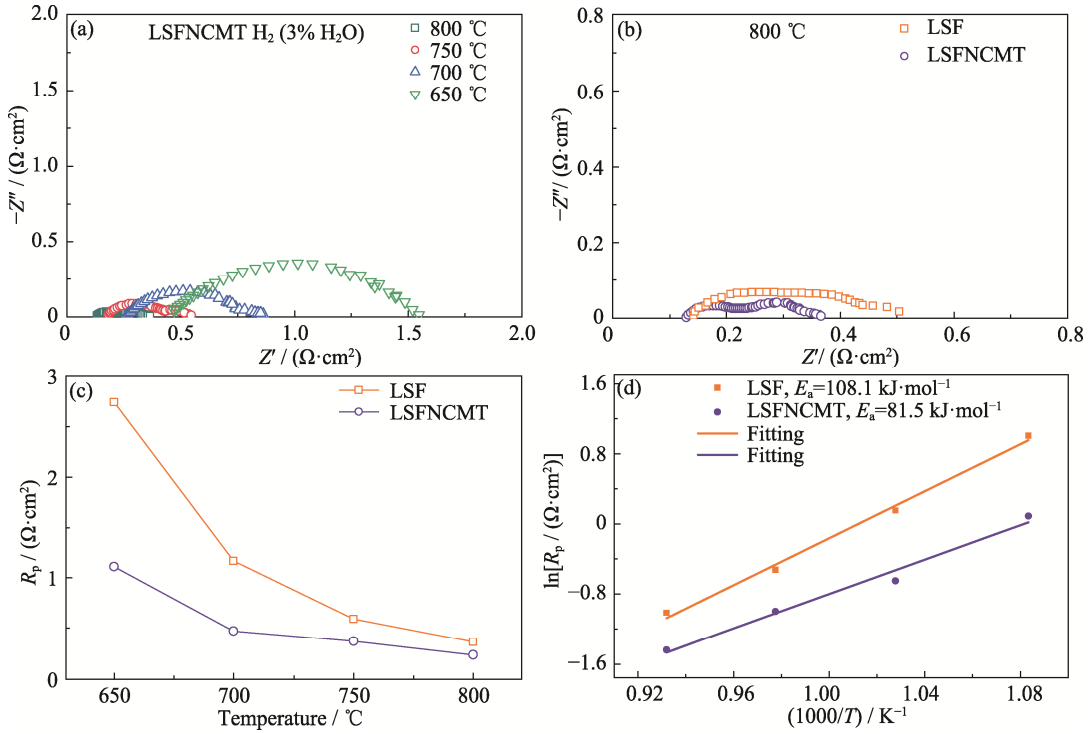

Fig. 7　Electrochemical performance of the anode-supported single cell at 650–800 ℃ in wet H_2 (3% (in volume) H_2O)
(a) EIS spectra of LSFNCMT cathode; (b) EIS spectra of LSF and LSFNCMT cathodes at 800 ℃; (c) R_p at different temperatures and (d) corresponding Arrhenius plots of different single cells

increasing temperature, but at the same temperature, the LSFNCMT exhibits a smaller R_p compared to the LSF (Fig. 7(b)). As shown in Fig. 7(c), R_p of the single cell at 650, 700, 750, 800 ℃ are 2.74, 1.17, 0.59, 0.36 Ω·cm^2 for LSF cathode, and 1.11, 0.47, 0.37, 0.24 Ω·cm^2 for LSFNCMT cathode, respectively. E_a of

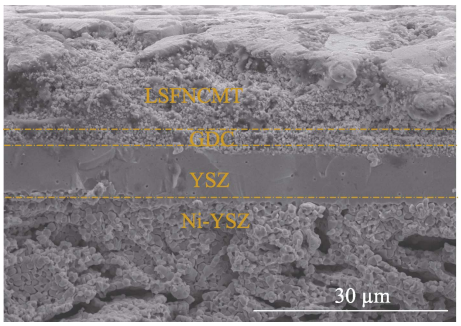

Fig. 8 Cross-sectional SEM image of single cell with LSFNCMT cathode

LSF (108.1 kJ·mol^{-1}) and LSFNCMT (81.5 kJ·mol^{-1}) single cells are calculated from R_p at different temperatures (Fig. 7(d)), indicating that high-entropy doping at the B-site significantly enhanced the ORR activity of LSF cathode materials.

Cross-sectional SEM images of LSF|GDC|LSF and LSFNCMT|GDC|LSFNCMT after testing are presented in Fig. S7. GDC electrolyte exhibits relatively high density, and the thickness of cathode material is approximately 20 μm. Cross-sectional SEM images of two single cells are shown in Fig. S8 and Fig. 8, respectively. The thicknesses of both electrolytes are around 12 μm without any evidence of cracking or detachment at the cathode/electrolyte and anode/electrolyte interfaces after testing. These results highlight that both half-cells and single cells of LSFNCMT cathode material and LSF cathode material exhibit good stability.

3 Conclusions

In this study, B-site high-entropy perovskite oxide $La_{0.7}Sr_{0.3}(FeNiCo)_{0.8}Mo_{0.1}Ti_{0.1}O_{3-\delta}$ is designed and used as the cathode material for SOFC. LSF and LSFNCMT exhibit excellent chemical compatibility with electrolyte GDC. At 800 ℃, R_p of the symmetric cell with LSFNMCT cathode (0.11 Ω·cm^2) is lower than that with LSF cathode (0.31 Ω·cm^2), indicating the superior ORR activity of LSFNCMT material. Furthermore, LSFNCMT exhibits superior chromium resistance compared to LSF, which can be attributed to the outstanding stability derived from the high-entropy design. The performance of single cell reveals that the B-position high-entropy design enhances catalytic activity of LSF material, resulting in a higher MPD of the single cell (1105.26 mW·cm^{-2} at 800 ℃) with R_p of 0.24 Ω·cm^2. In general, the high B-site entropy of LSF cathode improves the catalytic activity and chromium resistance, making it a promising candidate for SOFC applications.

Supporting materials

Supporting materials related to this article can be found at https://doi.org/10.15541/jim20240410.

References:

[1] PAN Z, LIU Q, NI M, *et al*. Activation and failure mechanism of $La_{0.6}Sr_{0.4}Co_{0.2}Fe_{0.8}O_{3-\delta}$ air electrode in solid oxide electrolyzer cells under high-current electrolysis. *International Journal of Hydrogen Energy*, 2018, **43(11):** 5437.

[2] CAOO D, ZHOU M, LIU Z, *et al*. Fabrication and characterization of anode-supported solid oxide fuel cell based on proton conductor electrolyte. *Journal of Inorganic Materials*, 2020, **35(9):** 1047.

[3] LAGUNA-BERCERO M A, CAMPANA R, LARREA A, *et al*. Electrolyte degradation in anode supported microtubular yttria stabilized zirconia-based solid oxide steam electrolysis cells at high voltages of operation. *Journal of Power Sources*, 2011, **196(21):** 8942.

[4] SINGH V, MUROYAMA H, MATSUI T, *et al*. Feasibility of alternative electrode materials for high temperature CO_2 reduction on solid oxide electrolysis cell. *Journal of Power Sources*, 2015, **293:** 642.

[5] LV H, ZHOU Y, ZHANG X, *et al*. Infiltration of $Ce_{0.8}Gd_{0.2}O_{1.9}$ nanoparticles on $Sr_2Fe_{1.5}Mo_{0.5}O_{6-\delta}$ cathode for CO_2 electroreduction in solid oxide electrolysis cell. *Journal of Energy Chemistry*, 2019, **35:** 71.

[6] YE Z, ZOU G, WU Q, *et al*. Preparation and performances of tubular cone-shaped anode-supported segmented-in-series direct carbon solid oxide fuel cell. *Journal of Inorganic Materials*, 2024, **39(7):** 819.

[7] XUE L, LI S, AN S, *et al*. Ca-doping cobalt-free double perovskite oxide as a cathode material for intermediate-temperature solid oxide fuel cell. *Molecules*, 2024, **29(13):** 2991.

[8] PRAŻUCH J, PYZALSKI M, FERNÁNDEZ GONZÁLEZ D, *et al*. Physicochemical properties of (La,Sr)CoO_3 thick films on Fe-25Cr steel under exposure to SOFC cathode operating conditions. *Materials*, 2024, **17(15):** 3791.

[9] PINSKY R, SABHARWALL P, HARTVIGSEN J, *et al*. Comparative review of hydrogen production technologies for nuclear hybrid energy systems. *Progress in Nuclear Energy*, 2020, **123:** 103317.

[10] DING P, LI W, ZHAO H, *et al*. Review on Ruddlesden-Popper perovskites as cathode for solid oxide fuel cells. *Journal of Physics: Materials*, 2021, **4(2):** 022002.

[11] GREELEY J, MARKOVIC N M. The road from animal electricity to green energy: combining experiment and theory in electrocatalysis. *Energy and Environmental Science*, 2012, **5(11):** 9246.

[12] SHEN R, NIE J, WANG K, *et al*. Applying multifunctional perovskite $LaNiO_3$ as electrolyte and anode for low‐temperature solid oxide fuel cell. *Journal of Materials Science: Materials in Electronics*, 2021, **32(4):** 4196.

[13] ZHANG K, WANG Y, ZHU T, *et al*. $LaNi_{0.6}Fe_{0.4}O_3$ cathode contact material: electrical conducting property manipulation and its effect on SOFC electrochemical performance. *Journal of Inorganic Materials*, 2024, **39(4):** 367.

[14] ZHANG Y, KNIBBE R, SUNARSO J, *et al*. Recent progress on advanced materials for solid-oxide fuel cells operating below 500 ℃. *Advanced Materials*, 2017, **29(48):** 1700132.

[15] ISTOMIN S Y, ANTIPOV E V. Cathode materials based on perovskite-like transition metal oxides for intermediate temperature solid oxide fuel cells. *Russian Chemical Reviews*, 2013, **82(7):** 686.

[16] ZHANG J, SONG K, GAO Y, *et al*. Tuning the thermo-mechanical synergies effect of solid oxide fuel cells with negative thermal expansion $NdMnO_3$ in $La_{0.6}Sr_{0.4}Co_{0.2}Fe_{0.8}O_{3-\delta}$-based symmetric electrode. *Chemical Engineering Journal*, 2024, **491:** 152063.

[17] CHEN Y, ZHU J, XIA T, *et al*. Improved electrocatalytic activity and CO_2 tolerance of iron-based perovskite as an intermediate temperature SOFC cathode. *Fuel*, 2024, **375:** 132546.

[18] XIA Z, ZHANG Y, XIONG X, *et al*. Realizing B-site high-entropy air electrode for superior reversible solid oxide cells. *Applied Catalysis B: Environmental*, 2024, **357:** 124410.

[19] JIN F, LIU X, TIAN Y, *et al*. Enhancing oxygen reduction activity and CO_2 tolerance by a bismuth doping strategy for solid oxide fuel cell cathodes. *Advanced Functional Materials*, 2024, **34(29):** 2400519.

[20] CHU Z, GAO J, LI Q, *et al*. Highly oxygen reduction activity and CO_2 resistance of Fe-based cathode electrocatalysts for solid oxide fuel cells. *Journal of Materials Science and Technology*, 2025, **212:** 303.

[21] ZHANG H X, YAO C G, ZHANG Z, *et al*. Lithium doping enhanced ORR kinetics and CO_2 tolerance of iron-based double perovskite cathode for solid oxide fuel cells. *Journal of Alloys and Compounds*, 2024, **980:** 173632.

[22] BAI J, NIU L, ZHU Q, *et al*. Ni-doped Fe-based perovskite to obtain multifunctional and highly efficient electrocatalytic active IT-SOFC electrode. *Fuel*, 2024, **365:** 131334.

[23] SUN C, SHEN Y, WANG F, *et al*. Optimization of a cobalt-free $La_{0.7}Sr_{0.3}FeO_{3-\delta}$-$BaZr_{0.1}Ce_{0.7}Y_{0.2}O_{3-\delta}$ composite cathode for proton-conducting solid oxide fuel cells. *Journal of Alloys and Compounds*, 2022, **923:** 166447.

[24] YANG C, WANG Z, TAN Y, *et al*. Interface engineering of $La_{0.6}Sr_{0.4}Co_{0.2}Fe_{0.8}O_{3-\delta}$/$Gd_{0.1}Ce_{0.9}O_{1.95}$ heterostructure oxygen electrode for solid oxide electrolysis cells with enhanced CO_2 electrolysis performance. *Chemical Engineering Journal*, 2024, **498:** 155461.

[25] WANG J, FU L, YANG J, *et al*. Cerium and ruthenium co-doped $La_{0.7}Sr_{0.3}FeO_{3-\delta}$ as a high-efficiency electrode for symmetrical solid oxide fuel cell. *Journal of Rare Earths*, 2021, **39(9):** 1095.

[26] YUAN M, WANG Z, GAO J, *et al*. Configuration entropy tailored beneficial surface segregation on double perovskite cathode with enhanced Cr-tolerance for SOFC. *Ceramics International*, 2024, **50(9):** 15076.

[27] ZHANG X, JIN Y, JIANG Y, *et al*. Enhancing chromium poisoning tolerance of $La_{0.8}Sr_{0.2}Co_{0.2}Fe_{0.8}O_{3-\delta}$ cathode by $Ce_{0.8}Gd_{0.2}O_{1.9-\delta}$ coating. *Journal of Power Sources*, 2022, **547:** 231996.

[28] HUANG K. A thermodynamic perspective on electrode poisoning in solid oxide fuel cells. *International Journal of Minerals, Metallurgy and Materials*, 2024, **31(6):** 1449.

[29] JIANG S P, ZHANG S, ZHEN Y D. Deposition of Cr species at (La, Sr)(Co, Fe)O_3 cathodes of solid oxide fuel cells. *Journal of the Electrochemical Society*, 2006, **153(1):** A127.

[30] GAO Y, HUANG X, YUAN M, *et al*. A $SrCo_{0.9}Ta_{0.1}O_{3-\delta}$ derived medium-entropy cathode with superior CO_2 poisoning tolerance for solid oxide fuel cells. *Journal of Power Sources*, 2022, **540:** 231661.

[31] GAO Y, LING Y, WANG X, *et al*. Sr-deficient medium-entropy $Sr_{1-x}Co_{0.5}Fe_{0.2}Ti_{0.1}Ta_{0.1}Nb_{0.1}O_{3-\delta}$ cathodes with high Cr tolerance for solid oxide fuel cells. *Chemical Engineering Journal*, 2024, **479:** 147665.

[32] LI Z, GE Y, XIAO Y, *et al*. Fabrication and performance investigation of high entropy perovskite $(Sr_{0.2}Ba_{0.2}Bi_{0.2}La_{0.2}Pr_{0.2})FeO_3$ IT-SOFC cathode material. *Journal of Alloys and Compounds*, 2024, **989:** 174357.

[33] GUO T M, DONG J B, CHEN Z P, *et al*. Enhanced compatibility and activity of high-entropy double perovskite cathode material for IT-SOFC. *Journal of Inorganic Materials*, 2022, **38(6):** 693.

[34] HAN X, LING Y, YANG Y, *et al*. Utilizing high entropy effects for developing chromium-tolerance cobalt-free cathode for solid oxide fuel cells. *Advanced Functional Materials*, 2023, **33(43):** 230478.

[35] WANG J, SACCOCCIO M, CHEN D, *et al*. The effect of A-site and B-site substitution on $BaFeO_{3-\delta}$: an investigation as a cathode material for intermediate-temperature solid oxide fuel cells. *Journal of Power Sources*, 2015, **297:** 511.

[36] KUAI X, YANG G, CHEN Y, *et al*. Boosting the activity of $BaCo_{0.4}Fe_{0.4}Zr_{0.1}Y_{0.1}O_{3-\delta}$ perovskite for oxygen reduction reactions at low-to-intermediate temperatures through tuning B-Site cation deficiency. *Advanced Energy Materials*, 2019, **9(38):** 1902384.

[37] ZHU C, LIU X, YI C, *et al*. Novel $BaCo_{0.7}Fe_{0.3-y}Nb_yO_{3-\delta}$ (y=0–0.12) as a cathode for intermediate temperature solid oxide fuel cell. *Electrochemistry Communications*, 2009, **11(5):** 958.

[38] ZHOU Q, WEI T, SHI Y, *et al*. Evaluation and optimization of $SrCo_{0.9}Ta_{0.1}O_{3-\delta}$ perovskite as cathode for solid oxide fuel cells. *Current Applied Physics*, 2012, **12(4):** 1092.

[39] SHEN Y, WANG F, MA X, *et al*. $SrCo_{1-y}Ti_yO_{3-\delta}$ as potential cathode materials for intermediate-temperature solid oxide fuel cells. *Journal of Power Sources*, 2011, **196(18):** 7420.

[40] ZHAO H, TENG D, ZHANG X, *et al*. Structural and electrochemical studies of $Ba_{0.6}Sr_{0.4}Co_{1-y}Ti_yO_{3-\delta}$ as a new cathode material for IT-SOFCs. *Journal of Power Sources*, 2009, **186(2):** 305.

[41] YU X, LONG W, JIN F, *et al*. Cobalt-free perovskite cathode materials $SrFe_{1-x}Ti_xO_{3-\delta}$ and performance optimization for intermediate-temperature solid oxide fuel cells. *Electrochimica Acta*, 2014, **123:** 426.

[42] LI J, SUN N, LIU X, *et al*. Investigation on $Nd_{1-x}Ca_xBaCo_2O_{5+\delta}$ double perovskite as new oxygen electrode materials for reversible solid oxide cells. *Journal of Alloys and Compounds*, 2022, **913:** 165245.

[43] CHEN Z P, JIN F J, LI M F, *et al*. Double perovskite $Sr_2CoFeO_{5+\delta}$: preparation and performance as cathode material for intermediate-temperature solid oxide fuel cells. *Journal of Inorganic Materials*, 2023, **39(3):** 337.

[44] ZHANG Z, WANG H, LI X, *et al*. CO_2/Cr-tolerance and oxygen reduction reaction of novel high-entropy perovskite cathode for intermediate temperature solid oxide fuel cell. *Ceramics International*, 2024, **50(7):** 11360.

[45] SCHULER J A, YOKOKAWA H, CALDERONE C F, *et al*. Combined Cr and S poisoning in solid oxide fuel cell cathodes. *Journal of Power Sources*, 2012, **201:** 112.

[46] LI Y, ZHANG W, ZHENG Y, *et al*. Controlling cation segregation in perovskite-based electrodes for high electro-catalytic activity and durability. *Chemical Society Reviews*, 2017, **46(20):** 6345.

[47] JEONG N C, LEE J S, TAE E L, *et al*. Acidity scale for metal oxides and Sanderson's electronegativities of lanthanide elements. *Angewandte Chemie International Edition*, 2008, **47(52):** 10128.

B 位高熵策略提高 $La_{0.7}Sr_{0.3}FeO_{3-\delta}$ 基阴极性能

刘弘明[1], 张金柯[2], 陈正鹏[1], 李明飞[1], 钱秀洋[1], 孙传骐[1],
熊 凯[3], 饶睦敏[1], 陈创庭[1], 高 源[2], 凌意瀚[2]

(1. 广东能源集团科学技术研究院有限公司, 广州 510000; 2. 中国矿业大学 材料与物理学院, 徐州 221116; 3. 广东省能源集团有限公司, 广州 510000)

摘 要: 作为经典的固体氧化物燃料电池(SOFC)阴极材料, 铁基钙钛矿材料具有成本低、热膨胀系数低和稳定性高的优点。本研究采用柠檬酸-硝酸盐燃烧法制备了 B 位高熵钙钛矿氧化物 $La_{0.7}Sr_{0.3}(FeNiCo)_{0.8}Mo_{0.1}Ti_{0.1}O_{3-\delta}$(LSFNCMT)。由于高熵材料的氧表面交换速率更快, LSFNCMT 阴极显示出优异的氧还原反应(ORR)活性, 800 ℃的极化电阻(R_p)为 0.11 Ω·cm^2, 远低于 LSF 阴极的 0.31 Ω·cm^2。更重要的是, 由于掺入高酸度的 Ni、Co 和 Mo 离子以及平均金属氧键能(ABE)更高的 Ti 离子, 高熵材料表现出更出色的稳定性。以 LSFNCMT 为阴极的对称电池在含铬气氛中进行 22 h 的稳定性测试, R_p 仅从 1.07 Ω·cm^2 增加到 2.98 Ω·cm^2, 而 LSF 对称电池的 R_p 从 2.62 Ω·cm^2 增加到 7.90 Ω·cm^2。LSFNCMT 阴极单电池在 800 ℃下的最大功率密度(MPD)为 1105.26 mW·cm^{-2}, 显著高于 LSF 阴极单电池(830.74 mW·cm^{-2}), 800 ℃下 R_p 为 0.24 Ω·cm^2, 也低于相同条件下 LSF 阴极单电池(0.36 Ω·cm^2), 证实高熵阴极具有卓越的耐毒化性。结果表明, B 位高熵是提高阴极材料催化活性和耐铬性的有效途径。

关 键 词: 固体氧化物燃料电池; 阴极材料; B 位高熵; 抗铬中毒

中图分类号: O61 **文献标志码:** A **文章编号:** 1000-324X(2025)12-1433-10

Supporting materials

Enhanced Performance of $La_{0.7}Sr_{0.3}FeO_{3-\delta}$ Cathode for SOFC *via* Implementation of B-site High-entropy Strategy

LIU Hongming[1], ZHANG Jinke[2], CHEN Zhengpeng[1], LI Mingfei[1], QIAN Xiuyang[1], SUN Chuanqi[1], XIONG Kai[3], RAO Mumin[1], CHEN Chuangting[1], GAO Yuan[2], LING Yihan[2]

(1. Guangdong Energy Group Science and Technology Research Institute Co., Ltd., Guangzhou 510000, China; 2. School of Materials Science and Physics, University of Mining and Technology, Xuzhou 221116, China; 3. Guangdong Energy Group Co., Ltd., Guangzhou 510000, China)

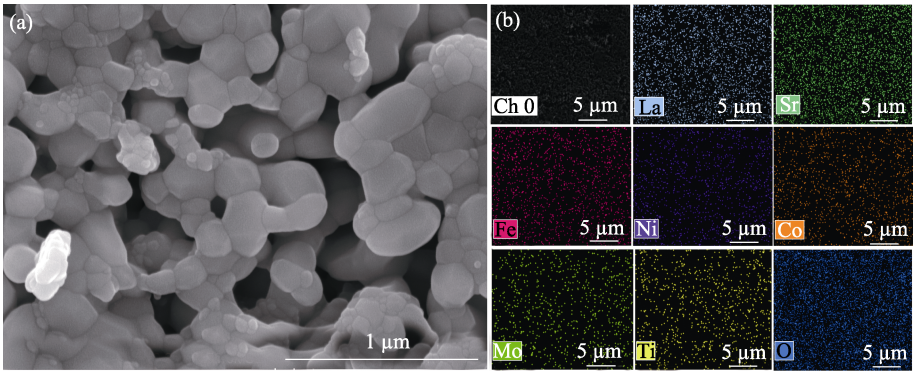

Fig. S1　SEM image (a) and corresponding EDS element mappings (b) of LSFNCMT

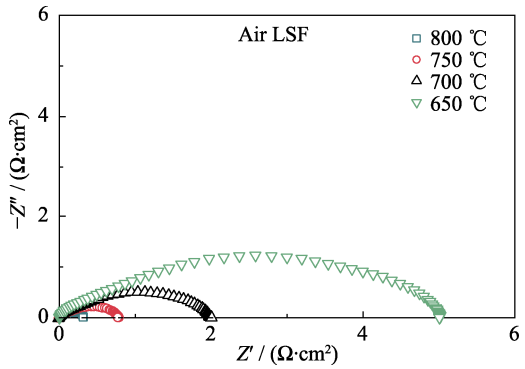

Fig. S2　EIS spectra of symmetric cell with LSF electrode in air at different temperatures

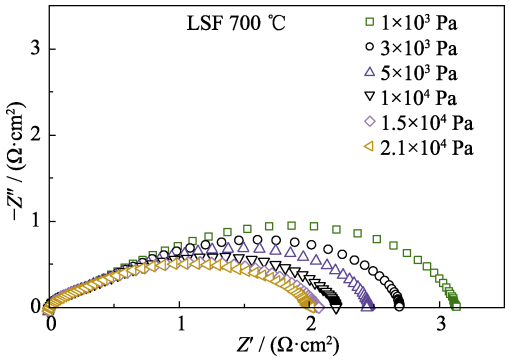

Fig. S3　EIS spectra of symmetric cell with LSF electrode under different $p(O_2)$ at 700 ℃

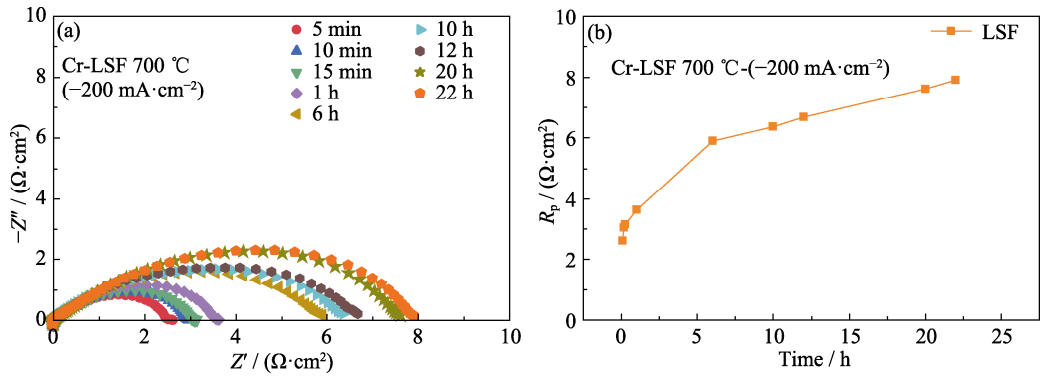

Fig. S4　EIS spectra (a) and variation of R_p (b) of symmetric cell with LSF electrode within 22 h in Cr vapor at –200 mA·cm^{-2} and 700 ℃

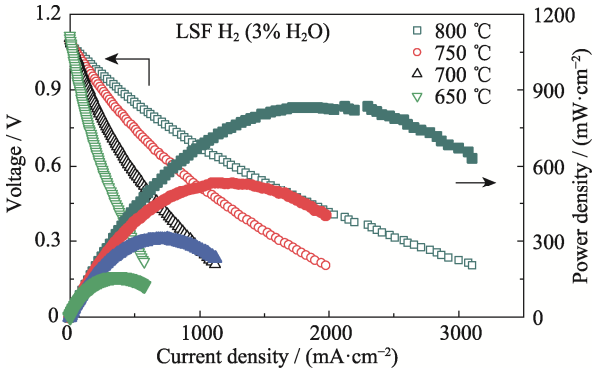

Fig. S5 *I–V* and power density curves of single cell with LSF cathode at 650–800 ℃ with wet H_2 (3% (in volume) H_2O)

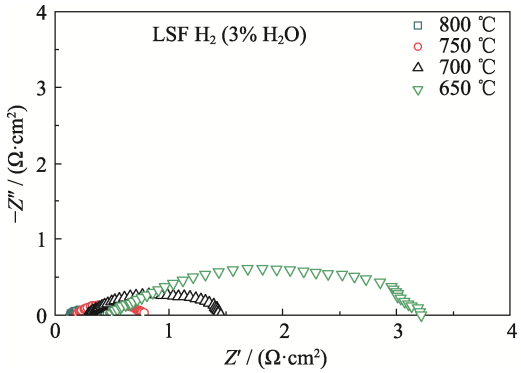

Fig. S6 EIS spectra of single cell with LSF cathode at 650–800 ℃ with wet H_2 (3% (in volume) H_2O)

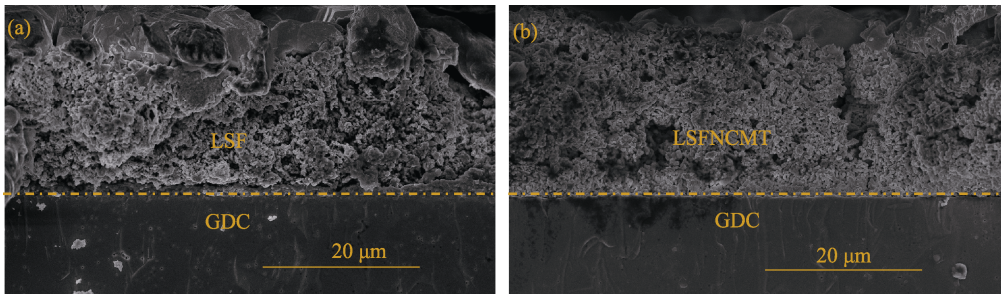

Fig. S7 Cross-sectional SEM images of symmetric cells with LSF (a) and LSFNCMT (b) electrodes

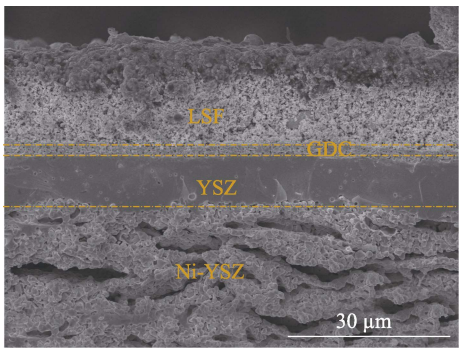

Fig. S8 Cross-sectional SEM image of single cell with LSF cathode